Impact of DIC biases on the selection process of a unique test for anisotropic plasticity characterization

Jean-David Thoby[1,2*], *Thomas* Fourest[1], *Bertrand* Langrand[1], *Delphine* Notta-Cuvier[2,3] and *Eric* Markiewicz[2]

[1]DMAS, ONERA, F-59014 Lille - France
[2]Univ. Polytechnique Hauts-de-France, LAMIH, CNRS, UMR 8201, 59313, Valenciennes, France
[3]INSA, Hauts-de-France, F59313 Valenciennes, France

Abstract. The exploitation of field measurements with inverse identification methods may reduce the number of required tests to characterize complex material constitutive models, provided that the generated stress field is sensitive enough to the targeted material parameters. For anisotropic elastoplastic material, the objective is to generate various stress states in the specimen through a single test. In this study, the effect of Digital Image Correlation measurement biases on the selection of the most suitable specimen geometry for characterisation of a complex anisotropic plasticity criterion using a unique uniaxial tensile test is investigated. To this aim, finite element (FE) based synthetic images are generated and DIC is used on these images. The biases in DIC measurement result in biased stress states that may cause errors in identification results.

1 Introduction

Commercial aviation industry is facing important challenges regarding the expectations about reduction of CO2 emissions. In addition to studies on propulsion systems, engineers are also focussing on reducing the weight of aircraft. This work involves manufacturing techniques, part design and selection of new lightweight materials. Each of these aspects relies on numerical predictions of aircraft structures behaviour. The quality of these simulations depends on the accuracy of constitutive laws for material behaviour modelling, which can be complex. For instance, several laminated aluminium alloys (*e.g.* AA2198-T351) show strong anisotropic behaviour that requires the definition and characterization of appropriate yield criteria [1].

Identifying the constitutive material parameters of these criteria with standard procedure requires numerous statically determined uniaxial tensile tests, performed in different loading directions with respect to the rolling direction of laminated materials. The accurate processing of such statically determined tests requires ensuring spatial homogeneity of stress field and strain rate during the tests.

* Corresponding author: jean-david.thoby@onera.fr

On the contrary, inverse identification methods such as the Virtual Fields Method (VFM) allow the exploitation of heterogeneous mechanical fields, which may significantly reduce the number of tests required for the identification of complex behaviour [2]. To identify the parameters of an anisotropic yield criterion through a single test, numerous stress states must be generated to involve all the constitutive parameters in the mechanical response. However, the design of such optimal specimen geometry remains an open problem [3].

Some geometries were suggested in the literature to expand the range of generated stress states but the impact of the biases introduced by full-field measurement in real conditions (noise, resolution, biased data close to the edges etc.) were not taken into account. This study aims to develop a numerical procedure to evaluate the impact of full field measurement during the selection process of the most suitable specimen geometry, i.e. leading to the generation of heterogeneous stress field with the broadest possible distribution over the yield surface. In the present study, the finites elements method is used to simulate tensile tests on four specimens. Then, a set of synthetic images is generated and Digital Image Correlation (DIC) is used to compute kinematic fields from these images. As a first step, the effect of biases introduced by DIC on the generated stress states is analysed by comparison of results from finite element simulations and from synthetic images.

2 Studied material

The studied material is an aluminium-copper-lithium alloy developed by Constellium. The main properties of this type of aluminium alloy are low density, good strength and resistance to mechanical damage [4]. The AA2198 is used in the aeronautic industry to manufacture commercial aircraft fuselage skin and components of the wings.

2.1 Constitutive model

First, the anisotropic elastoplastic behaviour of the AA2198-T351 alloy was characterized using several uniaxial tensile tests on standard specimens with different orientations with the respect to rolling direction.

The limits of the elastic domain (yield surface) is defined based on an equivalent stress σ_{eq}, which is calculated using the anisotropic yield criterion of Bron and Besson [5]. This yield criterion is able to simulate the angular variation of the initial yield stress, σ_0, and the Lankford coefficient, r, (ratio between longitudinal and trough-thickness plastic strain). The equivalent stress is the sum of two components (1), which are computed using the Eigen values of a linear transformation of the stress tensor (2,3,4). The equivalent stress, σ_{eq}, depends on parameters a, b^1 and b^2 that control the global shape of the yield surface and the parameters c_j^i, which control the anisotropy, deform the yield surface in a specific direction. The hardening is modelled using a power law, dependent on two parameters K and n (5). The identified parameters for the AA2198-T351 are reported in **Table 1** and the associated material behaviour is presented in **Fig. 1** and **Fig. 2**.

$$\left(\alpha\left(\sigma_{eq}^1\right)^a + (1-\alpha)\left(\sigma_{eq}^2\right)^a\right)^{1/a} = \sigma_{eq} \tag{1}$$

$$\sigma_{eq}^1 = \left(\frac{1}{2}\left(\left|\tilde{S}_2^1 - \tilde{S}_3^1\right|^{b^1} + \left|\tilde{S}_3^1 - \tilde{S}_1^1\right|^{b^1} + \left|\tilde{S}_1^1 - \tilde{S}_2^1\right|^{b^1}\right)\right)^{1/b^1} \tag{2}$$

$$\Phi^2 = \left(\frac{3^{b^2}}{2^{b^2}+2}\left(\left|\tilde{S}_1^2\right|^{b^2} + \left|\tilde{S}_2^2\right|^{b^2} + \left|\tilde{S}_3^2\right|^{b^2}\right)\right)^{1/b^2} \tag{3}$$

$$\bar{\bar{S}}^k = \frac{1}{3}\begin{bmatrix} c_2^k + c_3^k & -c_3^k & -c_2^k & 0 & 0 & 0 \\ -c_3^k & c_3^k + c_1^k & -c_1^k & 0 & 0 & 0 \\ -c_2^k & -c_1^k & (c_1^k + c_2^k)/3 & 0 & 0 & 0 \\ 0 & 0 & 0 & 3c_4^k & 0 & 0 \\ 0 & 0 & 0 & 0 & 3c_5^k & 0 \\ 0 & 0 & 0 & 0 & 0 & 3c_6^k \end{bmatrix} : \bar{\sigma} \tag{4}$$

$$\sigma_y = \sigma_0 + K(1 - e^{-n\varepsilon_p}) \tag{5}$$

Table 1. Identified material parameters for the AA2198-T351

E [GPa]	υ [ ]	σ_0 [MPa]	K [MPa]	n [ ]
73.3	0.31	324.42	223.79	14.81
a [ ]	α [ ]	b^k [ ]		
19.9994	0.9989	a		
c_1^1 [ ]	c_2^1 [ ]	c_3^1 [ ]	c_4^1 [ ]	$c_{5,6}^1$ [ ]
1.2503	1.2622	0.5217	1.2453	1
c_1^2 [ ]	c_2^2 [ ]	c_3^2 [ ]	c_4^2 [ ]	$c_{5,6}^2$ [ ]
1.0890	0.7497	2.0327	1.9739	1

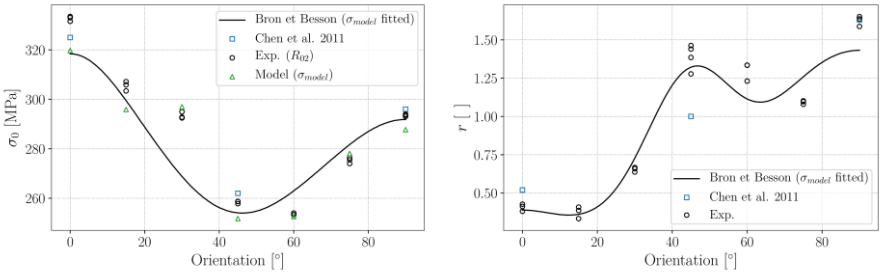

Fig. 1. Angular variation of the initial yield stress (left) and of the Lankford coefficient (right)

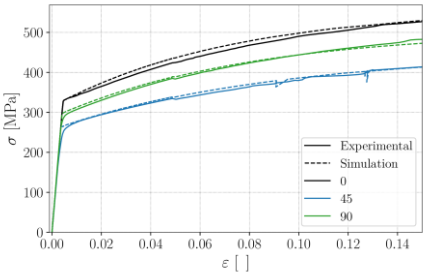

Fig. 2. Experimental and numerical stress/strain curves for three orientations

3 Heterogeneous tensile tests simulations

3.1 Tested geometries

Regardless of the employed identification method, the identification result relies on the sensitivity of the stress fields to each material parameter. Therefore, the ideal test to identify the parameters of an anisotropic yield criterion should generate heterogeneous stress fields

involving uniaxial and biaxial traction, uniaxial and biaxial compression and pure and simple shear, going beyond the elastic limit in all cases, over a unique specimen loaded using a conventional test device.

In the last decade, multiple geometries have been designed to achieve this objective; the present study focuses on specimen geometries adapted to uniaxial tensile loadings. For instance, Marek et al. tested a notched specimen [6], Kim et al and Jones and al. designed more complex geometries: a "∑"-shape and a "D"-shape [7,8]. Finally, Barroqueiro et al. used topological optimization to generate a more complex specimen shape [9]. The present work focusses on the notched specimen only.

3.2 FEM model

To simulate tensile tests and analyse the stress states generated in the elements that reach plasticity, we uses the *Z-set* finite element software. The material behaviour is modelled using the constitutive equations and the associated material parameters identified previously. All simulation are performed using plane stress hypothesis. The elements are linear triangular shells with full integration with an average size of 0.5mm. The simulation stops when an element reach an equivalent plastic strain, ε_p, of 0.15.

3.3 Synthetic images generation and DIC

To take into account biases encountered with full-field measurement, synthetic test images are generated based on the finites elements simulations. The algorithm initially implemented by Bouda et al [10] uses the position of the pixel inside the deformed element (x_d, y_d). Then, it projects the pixel in the reference configuration (x_0, y_0) using isoparametric coordinates (ξ_i, η_i) of the pixel inside the element to define its grey level (**Fig. 3**). In this study, the grey level of the pixel is interpolated from the grey levels of a set of real pictures of a speckle pattern. The deformed pictures have been taken in the same configuration as for real tests (lightening, camera and pattern application technique). This helps makes synthetic images closer to real images considering the greys levels range and the sensor noise.

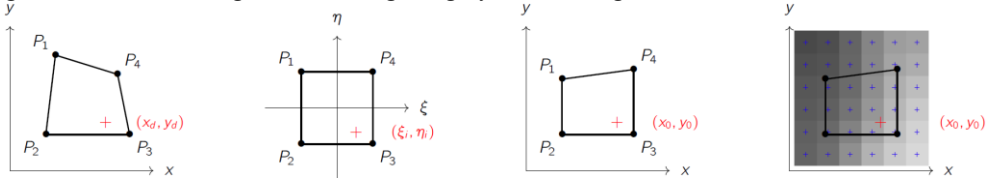

Fig. 3. Principle of finite element based image deformation process

The next step is to compute the displacement fields using a DIC software. In this study, the algorithm folkiD, developed by ONERA [11] is used. The strain fields are smoothed spatially and temporally using Gaussian filters with a window size of 20 pixels for spatial smoothing and 3 time steps for temporal smoothing. Finally the data close to the edge (less than the half of the smoothing window) is reconstructed by extension of the latest know value. The stress field and the equivalent plastic strain are obtained by calling the same routine than in the FEM model using the *Zmat* tool.

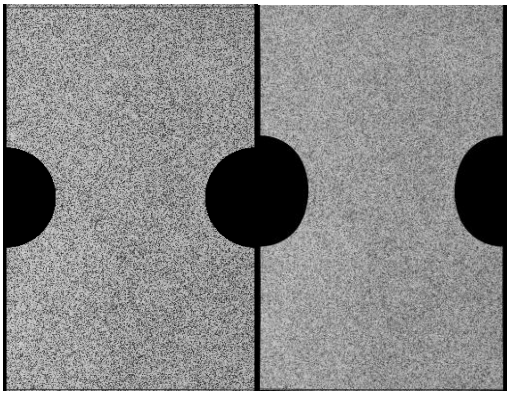

Fig. 4. Synthetic images of a tensile test on a deep-notched specimen (initial and deformed stages) simulating images with spatial resolution of 4320 x 2868 pixels

4 Results

To analyse the heterogeneity of the stress field from FE results, the generated stress states are projected on the yield surface. **Fig. 5** shows the equivalent plastic strain and the projection of the stress states over the yield surface computed by FE simulations at the final time step. The elements where the equivalent plastic strain is zero are coloured in light grey and the stress states inside those elements is not projected on the yield surface. The numerical simulations shows that a notched specimen can generate uniaxial tension and stress states close to biaxial tension and simple shear in elements that reach plasticity.

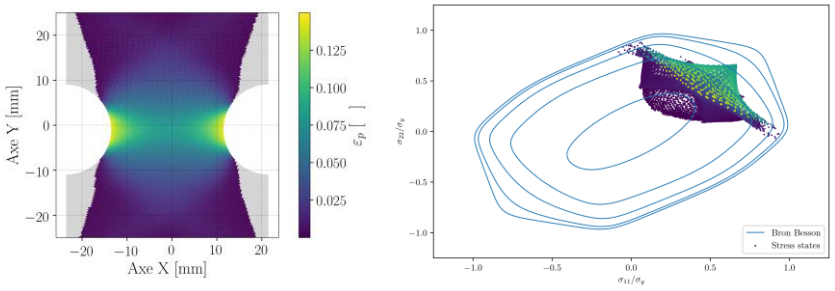

Fig. 5. Cumulated plastic strain field and stress states for a notched specimen

The same analysis is presented for the synthetic images of the notched specimen (**Fig. 6**) after computing the stress fields with the DIC results (i.e. including measurement biases). At the same time step, the regions that reach plasticity are the same than the reference FE simulation, except close to the edges, where reconstructed data generates plasticity while the simulation does not. The stress states thus obtained, in the region where the plastic strain is greater than 0.01, are similar to FE simulation ones, i.e., are mainly characteristics of uniaxial tension, with a tendency of expansion towards biaxial tension and simple shear. The inclusion of full-field measurement biases on synthetic images leads to the computation of stress states between pure and simple shear, which are not present in the reference FE simulation. As they are not real mechanical states, these biased stress states can cause errors in identification of the material parameters.

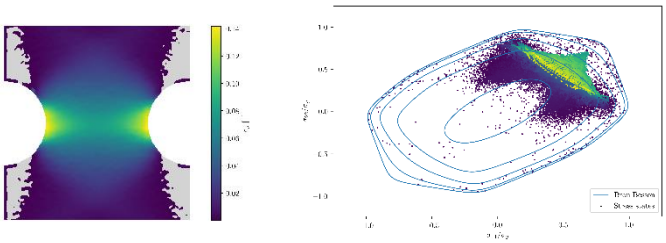

Fig. 6. Cumulated plastic strain field and stress states for the notched specimen computed from DIC results on synthetic images

A quantification of the biases induced by the measurement can be computed from the quantification of the mechanical field heterogeneity. A first approach can be based on the exploitation of strain fields, following the indicator suggested by Souto et al. (6) [12]. On the one hand, the strain states heterogeneity is expressed with the standard deviation, $\mathrm{Std}(\boldsymbol{\varepsilon_2}/\boldsymbol{\varepsilon_1})$, and the range, $(\boldsymbol{\varepsilon_2}/\boldsymbol{\varepsilon_1})_R$, of the ratio between minor and major strain. On the other hand, the range of plastic strain is analysed with its standard deviation, $\mathrm{Std}(\varepsilon_p)$, its average value, $Av(\varepsilon_p)$, and the maximum plastic strain reached for specific loadings (7). Each element is normalized by an absolute coefficient, w_{ai}, and weighted by a relative coefficient, w_{ri}. The coefficient values used in this work are reported in **Table 2**.

The results of the heterogeneity indicator and its components are reported in **Table 3**. Concerning the strain state ratio, DIC results increases the standard deviation. Moreover, some pixels with a major strain close to zero have caused the strain ratio range to explode. As this value is much higher than the other elements, it may not be relevant for computation of I_T with experimental results. Therefore, the relative coefficient w_{r2} was set to zero. The results also show that the maximum value of equivalent plastic strain has decreased. This is mainly due to the measurement biases close to the edges that underestimate the deformation (extension of the last know value). Also the shear observed with the synthetic images (**Fig. 6**) is reflected by the increase in the coefficient ${\varepsilon_p}^{\mathrm{Max}}_{\mathrm{shear}}$. Finally, for the same test, the value of the heterogeneity indicator has significantly increased. So it is possible to quantify the measurement biases using its variation.

$$I_T = w_{r1}\frac{\mathrm{Std}\left(\boldsymbol{\varepsilon_2}/\boldsymbol{\varepsilon_1}\right)}{w_{a1}} + w_{r2}\frac{\left(\boldsymbol{\varepsilon_2}/\boldsymbol{\varepsilon_1}\right)_R}{w_{a2}} + w_{r3}\frac{\mathrm{Std}(\varepsilon_p)}{w_{a3}} + w_{r4}\frac{{\varepsilon_p}^{\mathrm{Max}}}{w_{a4}} + w_{r5}\frac{Av(\varepsilon_p)}{w_{a5}} \quad (6)$$

$${\varepsilon_p}^{\mathrm{Max}} = \frac{{\varepsilon_p}^{\mathrm{Max}}_{\mathrm{test}} + {\varepsilon_p}^{\mathrm{Max}}_{\mathrm{tensile}} + {\varepsilon_p}^{\mathrm{Max}}_{\mathrm{shear}} + {\varepsilon_p}^{\mathrm{Max}}_{\mathrm{plane}} + {\varepsilon_p}^{\mathrm{Max}}_{\mathrm{biax.}} + {\varepsilon_p}^{\mathrm{Max}}_{\mathrm{comp.}}}{6} \quad (7)$$

Table 2. Coefficients used to compute the heterogeneity indicator

w_{r1}	w_{r2}	w_{r3}	w_{r4}	w_{r5}
0.3	0.0	0.2	0.4	0.1
w_{a1}	w_{a2}	w_{a3}	w_{a4}	w_{a5}
1	4	0.25	0.15	0.15

Table 3. Values of the heterogeneity indicator and its components for the notched specimen

	$\mathrm{Std}(\boldsymbol{\varepsilon_2}/\boldsymbol{\varepsilon_1})$	$(\boldsymbol{\varepsilon_2}/\boldsymbol{\varepsilon_1})_R$	$\mathrm{Std}(\boldsymbol{\varepsilon_p})$	${\boldsymbol{\varepsilon_p}}^{\mathrm{Max}}_{\mathrm{test}}$	${\boldsymbol{\varepsilon_p}}^{\mathrm{Max}}_{\mathrm{tensile}}$	${\boldsymbol{\varepsilon_p}}^{\mathrm{Max}}_{\mathrm{shear}}$	${\boldsymbol{\varepsilon_p}}^{\mathrm{Max}}_{\mathrm{plane}}$	${\boldsymbol{\varepsilon_p}}^{\mathrm{Max}}_{\mathrm{biax.}}$	${\boldsymbol{\varepsilon_p}}^{\mathrm{Max}}_{\mathrm{comp.}}$	$\boldsymbol{Av(\varepsilon_p)}$	$\boldsymbol{I_T}$
FE	0.240	0.775	0.029	0.150	0.017	0.0	0.119	0.0	0.0	0.022	0.237
DIC	0.668	104.0	0.031	0.142	0.020	0.014	0.126	0.0	0.009	0.030	0.383

5 Conclusions and future work

In this study, the objective was to quantify the influence of DIC measurement biases on the selection procedure of a specimen geometry to identify material parameters of an anisotropic yield criterion. To that end, synthetic images are used to investigate the effect of DIC measurement biases on the stress states range and on strain-based indicators. It reveals that the use of DIC can be the source of several biases that may affect the indicators for the selection of a heterogeneous states and the identification results, especially the occurrence of biased stress states.

Future work will aim at consolidating the use of criteria to quantify measurement induced biases. Then, this method will be used on several specimen geometries to compare their robustness to measurement biases. Then, real tests will be performed with several geometries to validate the selection procedure described in this paper.

Acknowledgement

The authors are grateful to ONERA and the Région Hauts-de-France for cofunding this project. Also, the authors would like to express our sincere gratitude to Constellium for supporting this study by providing the tested aluminum sheet.

1. D. Banabic, Plastic Behaviour of Sheet Metal (2010)
2. F. Pierron, M. Grédiac, The Virtual Fields Method (2012)
3. F. Pierron, M. Grédiac, Strain **57**, 1, e12370 (2021)
4. J. Chen, Y. Madi, T. F. Morgeneyer, J. Besson, Comput. Mat. Sci., **50**, 1365-1371 (2011)
5. F. Bron, J. Besson, Int. J. Plasticity, **20**, 937-963 (2004)
6. A. Marek, F. M. Davis, M. Rossi and F. Pierron, Int. J. Mat. Forming. **12**, 457–476 (2019)
7. J.-H Kim, F. Barlat, F. Pierron, M.-G. Lee, Exp. Mech., **54**(7), 1189–1204 (2014)
8. E. M. C. Jones, J. D. Carroll, K. N. Karlson, S. L. B. Kramer, R. B. Lehoucq, P. L. Reu, D. Z. Turner, Comput. Mat. Sci., **152**, 268–290 (2018)
9. B. Barroqueiro, A. Andrade-Campos, J. Dias-de Oliveira, R. A. F. Valente, Int. J. Mech. Sci., **181** (2020).
10. P. Bouda, B. Langrand, D. Notta-Cuvier, et al, Comput. Mech., **64**, 1639–1654 (2019)
11. G. Le Besnerais, Y. Le Sant, D. Lévêque, Strain, **52**, 286– 306 (2016)
12. N. Souto, S. Thuillier, A. Andrade-Campos, Int. J. Mech. Sci., **101–102**, 252-271 (2015).